Ultrathin pseudomorphic Sn/Si and Sn_xSi_{1-x}/Si heterostructures

Kyu Sung Min and Harry A. Atwater
Thomas J. Watson Laboratory of Applied Physics, California Institute of Technology, Pasadena, California 91125

(Received 24 October 1997; accepted for publication 16 February 1998)

Ultrathin, coherently strained Sn/Si and Sn_xSi_{1-x}/Si alloy quantum well structures with substitutional Sn incorporation far in excess of the equilibrium solubility limit have been fabricated via substrate temperature and growth flux modulations in molecular beam epitaxy. Sn/Si single and multiple quantum wells with Sn coverage up to 1.3 ML, $Sn_{0.05}Si_{0.95}$/Si multiple quantum wells of up to 2.0 nm, and $Sn_{0.16}Si_{0.84}$/Si multiple quantum wells of up to 1.1 nm are determined to be pseudomorphic, and coverage-dependent Sn segregation dynamics are observed. © *1998 American Institute of Physics.* [S0003-6951(98)03315-4]

One approach for realization of a direct energy-gap group IV alloy system involves alloying Sn with Si or Ge to form epitaxially stabilized diamond cubic Sn_xGe_{1-x}/Ge and Sn_xSi_{1-x}/Si heterostructures. Diamond cubic α-Sn is a zero-band-gap semiconductor with degenerate conduction and valence bands at the Γ point,[1] and band-structure calculations have suggested that when Si or Ge is alloyed with Sn, the resulting alloy systems Sn_xSi_{1-x} and Sn_xGe_{1-x} are predicted to have direct and tunable energy gaps for Sn compositions exceeding some critical concentration.[2,3] Recently, the indirect-to-direct band-gap transition was observed in Sn_xGe_{1-x} alloys.[4] While growth of dilute ($x<0.06$) pseudomorphic Sn_xSi_{1-x} alloy films has been previously demonstrated,[5,6] we report in this letter the growth of coherently strained, epitaxially stabilized thin quantum well heterostructures based on Sn/Si and Sn_xSi_{1-x}/Si with high x via temperature and growth rate modulations in molecular beam epitaxy. Growth of such heterostructures is motivated by the intuition that a Sn_xSi_{1-x} alloy has to be high in Sn concentration for realization of tunable direct band-gap material;[2,3] one might also potentially take advantage of the quantum carrier confinement to further tune the energy gap in α-Sn/Si and high Sn concentration Sn_xSi_{1-x}/Si quantum well heterostructures[7] over a wide range in the infrared frequency range.

Growth of such heterostructures is challenged by the large lattice mismatch between α-Sn and Si (19.5%), very low solid solubility of Sn in crystalline Si ($\sim 5\times10^{19}$ cm^{-3}),[8] and pronounced Sn segregation to the surface during growth at ordinary Si epitaxy temperatures ($T>\sim$400 °C). To incorporate Sn at high fractions while maintaining a high epitaxial quality, we employ temperature and growth rate modulations in molecular beam epitaxy, as previously used for growing Sb delta-doped layers in Si (Ref. 9) and Ge/α-Sn heterostructures on Ge.[10]

All samples were grown in a custom-built molecular beam epitaxy system with a base pressure of 3×10^{-10} Torr. The (100) Si substrates were prepared by first cleaning a 100 nm thermal oxide-coated wafer in 5:1:1 H_2O:H_2O_2:NH_4OH solution followed by subsequent complete removal of the oxide in a 10% HF–H_2O solution to obtain a hydrogen-terminated Si (100) surface. After transfer to ultrahigh vacuum, the substrates were baked *in situ* at 200 °C for 2 h to desorb hydrocarbon contaminants. Just prior to growth of the Si buffer layer, the substrates were heated to 550 °C to desorb hydrogen and obtain a (2×1) surface reconstruction. Si and Sn were deposited by electron-beam evaporation and thermal effusion, respectively. The Si deposition rate was controlled using a quartz-crystal monitor and the Sn deposition rate was controlled via effusion cell temperature. The Sn effusion cell temperature was varied between 675–755 °C to yield deposition rates between 0.003 and 0.02 monolayers (ML)/s (1 ML$=6.79\times10^{14}$ cm^{-2}). For all samples, the Si buffer layers were grown at 550 °C at 0.05 nm/s to obtain a smooth Si surface, as judged by reflection high-energy electron diffraction (RHEED) prior to deposition of the Sn or Sn_xSi_{1-x} layers. For Sn/Si growth, Sn deposition at 0.02 ML/s immediately followed Si buffer layer growth at 550 °C. The Sn-induced reconstructions observed by RHEED were in agreement with previous observations:[11] (6×2) for 0.375–0.5 ML, $c(4\times8)$ for 0.5–1.0 ML, (5×1) for 1.0–1.5 ML, and (5×1) plus streaks for coverages exceeding 1.5 ML. After Sn deposition, the growth was interrupted to cool the substrate to 130–170 °C, which took 15–30 min. To cap the Sn layer with minimal Sn segregation to the surface, Si overlayer growth at 130–170 °C was performed initially at 0.01–0.03 nm/s. The low initial growth rate is required to maximize the Si overlayer thickness prior to defect formation or a crystal-to-amorphous transition. The critical thickness h_{epi} at which epitaxial Si films undergo a crystal-to-amorphous transition is reportedly governed by an Arrhenius temperature dependence, and a growth rate dependent activation energy that yields larger h_{epi} for lower growth rates.[11] Another constraint on the Si overlayer grown at low temperatures is that it be thick enough to incorporate the deposited Sn. After 4–6 nm of Si overlayer deposition, the substrate temperature is increased so as to return the substrate temperature to 550 °C at an overlayer thickness of about 15 nm. At this point, the growth rate is also increased back to 0.05 nm/s. After further growth of the Si overlayer to a desired thickness, the process is repeated for multilayer samples. The growth procedure for Sn_xSi_{1-x}/Si was similar except that the growth was interrupted after deposition of the Si buffer layer to cool the substrate to 140–170 °C prior to

 © 1998 American Institute of Physics
Downloaded 31 Aug 2006 to 131.215.240.9. Redistribution subject to AIP license or copyright, see http://apl.aip.org/apl/copyright.jsp

TABLE I. Summary of incorporated Sn vs Sn segregated to the surface per buried layer.

Sample	Temp. (°C)	Initial Sn coverage per layer (ML)	Fraction segregated
(i) Single Sn/Si	170 °C	0.52,[a] 1.0[a]	<0.05
		1.4	0.09
		1.7	0.23
		2.2	0.52
(ii) Multiple Sn/Si	130 °C	1.3[a]	<0.02
	120 °C	2.1[b]	0.32
(iii) Multiple 2.0 nm $Si_{1-x}Sn_x$/Si	140 °C	0.30,[a] 0.76,[a] 1.5[b] (x=0.02,[a] 0.05,[a] 0.10[b])	<0.02
(iv) Multiple 1.1 nm $Si_{1-x}Sn_xSi$	110 °C	0.74,[a] 1.5,[a] 1.9[b] (x=0.10,[a] 0.16,[a] 0.25[b])	<0.02

[a]Determined to be pseudomorphic by cross-sectional TEM.
[b]Determined to be at least partially relaxed by cross-sectional TEM.

deposition of the Sn_xSi_{1-x} layers. Si overlayer growth followed Sn_xSi_{1-x} layer growth without growth interruption. Due to low growth temperature, only diffuse (2×1) Si reconstruction lines were visible during the deposition of alloy layers.

Samples were analyzed by cross-sectional transmission electron microscopy (TEM), Rutherford backscattering spectrometry (RBS), and high-resolution x-ray rocking curve analysis. Four types of sample configurations were investigated: (i) single 0.49–1.4 ML Sn layers sandwiched between Si, with 140–170 nm Si cap layers (single Sn/Si quantum well structures); (ii) multiple 1.3 ML Sn layers sandwiched between Si, with 115 nm Si spacer and cap layers (multiple Sn/Si quantum well structures); (iii) multiple 2 nm Sn_xSi_{1-x} (x=0.02, 0.05, and 0.10) layers sandwiched between Si with 80 nm Si spacer and cap layers (multiple Sn_xSi_{1-x}/Si quantum well structures); and (iv) multiple 1.1 nm Sn_xSi_{1-x} (x=0.10, 0.16, and 0.25) layers sandwiched between Si with 80 nm Si spacer and cap layers (multiple Sn_xSi_{1-x}/Si quantum well structures).

The four types of structures analyzed are summarized in Table I. The superscripts indicate whether the samples have been determined to be pseudomorphic (dislocation density $<1\times10^6$ cm^{-2}) within the analyzed electron-transparent area by cross-sectional transmission electron microscopy analysis. Table I also gives a summary of incorporated Sn versus Sn segregated to the surface per buried layer, as determined from Rutherford backscattering spectrometry. For Sn/Si structures, the temperature indicated is the temperature at which the initial Si overlayer was deposited after the Sn layer was deposited. For Sn_xSi_{1-x}/Si structures, the indicated temperature is the temperature at which the alloy layer and a subsequent thin Si overlayer was deposited. For all Sn_xSi_{1-x}/Si multiple well structures, the fraction of Sn segregated to the surface was low (<2%). For Sn/Si structures, the segregated fraction increases sharply above a critical initial coverage of about 1.4 ML. It is noteworthy that this coverage coincides with the predicted thickness for completion of the (5×1) surface reconstruction phase by Baski

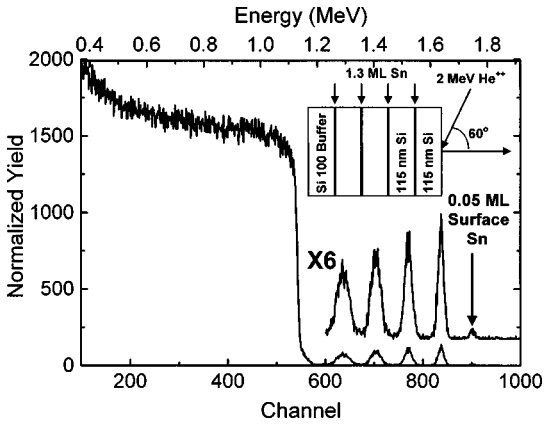

FIG. 1. Rutherford backscattering spectrum of a multiple Sn/Si quantum well structure with four periods of 1.3 ML Sn layers sandwiched between 115 nm Si spacer layers.

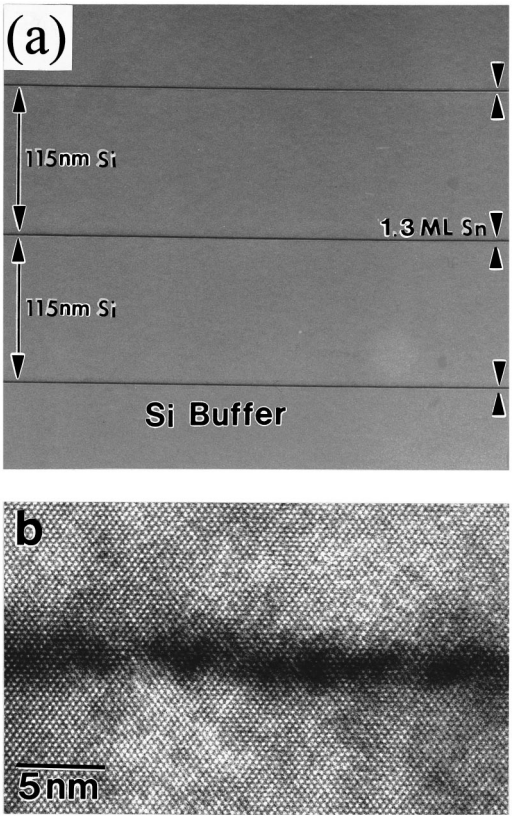

FIG. 2. Cross-sectional transmission electron micrographs of sample in Fig. 1. (a) Bright-field image taken under (400) two-beam excitation showing the first three Sn layers. (b) High-resolution image in the [110] projection of one of the Sn layers.

Downloaded 31 Aug 2006 to 131.215.240.9. Redistribution subject to AIP license or copyright, see http://apl.aip.org/apl/copyright.jsp

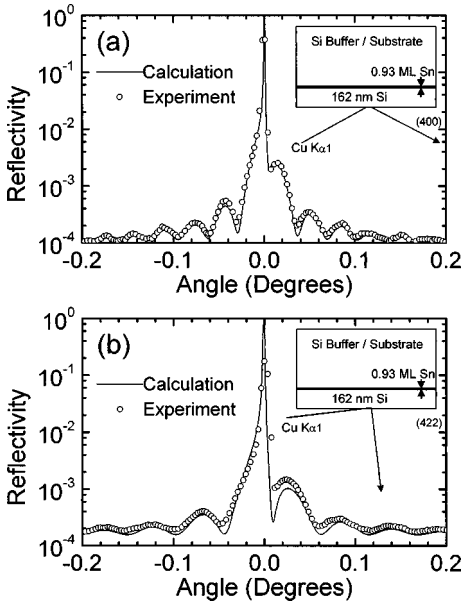

FIG. 3. (a) Symmetric (400) reflection and (b) asymmetric (422) reflection x-ray rocking curves of a single Sn/Si quantum well structure with 0.93 ML Sn sandwiched between Si with 162 nm Si cap layer, as determined by Rutherford backscattering spectrometry. The dotted curves represent the experimental data and the solid curves represent dynamical simulations for 0.15 nm Sn capped with 163 nm.

et al.[12] who viewed the (5×1) phase as a half-complete layer of Sn dimers over a complete $c(4\times8)$ phase of a monolayer of symmetrically dimerized Sn. The fact that islanding follows the (5×1) phase suggests that it may become more energetically favorable to relieve the surface strain by means of segregating Sn in excess of a complete (5×1) phase ($\sim$1.4 ML) to the surface even at such low temperatures.

Figure 1 shows the Rutherford backscattering spectrum of a multiple Sn/Si quantum well structure with four periods of 1.3 ML Sn layers sandwiched between 115 nm Si spacer layers. The large scattering cross section of Sn and the large relative mass ratio between Sn and Si enable very accurate measurements of the absolute Sn coverage. The increased energy width in the spectrum at increased depth is primarily due to He^{++} ion energy straggling. Within the resolution of RBS, no significant interdiffusion was observed, despite anneals at temperatures far exceeding the melting temperature of Sn.

Figure 2 shows cross-sectional transmission electron micrographs of the sample described in Fig. 1. Figure 2(a) is a bright-field image taken under (400) two-beam excitation showing the first three layers. The interfaces are sharp, with no dislocations or stacking faults. Figure 2(b) is a high-resolution image in the [110] projection of one of the layers shown in Fig. 2(a). No growth-related defects were visible within the analyzed region ($\sim$50 μm into the sample). The Sn layers in both images appear thicker due to strain contrast below and above each buried Sn; nonetheless, it is evident in Fig. 2(b) that most of the incorporated Sn is localized within a few atomic layers.

Single Sn/Si quantum well structures with Sn layers of 0.49 ± 0.09, 0.93 ± 0.09, and 1.3 ± 0.1 ML sandwiched between Si with 140–170 nm Si cap layers were analyzed using x-ray rocking curve analysis. Figures 3(a) and 3(b) show representative x-ray rocking curves of symmetric (400) and asymmetric (422) reflections, respectively. The dotted curves represent experimental data for the film with a single layer of 0.93 ± 0.09 ML Sn capped with 162 nm of Si, as determined by RBS. The solid curves represent dynamical simulations for a model film with 0.15 nm Sn capped with 163 nm Si. The simulations were performed under the assumption of a tetragonally distorted α-Sn unit cell with the bulk lattice constant of 0.64890 nm (in-plane lattice constant of 0.54310 nm and perpendicular lattice constant of 0.73875 nm) and bulk elastic constants. Several features about the interference fringes are noteworthy. The angular distance between Pendellosung fringes is independent of the physical properties of the sandwiched layer. However, the angular position and the intensity of the interference fringes near the (400) Si reflection depend strongly on the factors that cause dephasing of x rays scattered from the Si cap layer and the Si substrate. Because of the large atomic size difference between Sn and Si, analysis of the angular position and the intensity of the interference fringes offer a very sensitive technique for quantitatively characterizing low-coverage Sn incorporation, enabling thickness resolution within a fraction of a monolayer. As can be seen in Figs. 3(a) and 3(b), the interference fringes of the simulation curves match that of the experimental curves very well. The best values of Sn thickness determined from the dynamical x-ray simulation for (400) symmetric reflections of films with Sn coverages of 0.49 ± 0.09, 0.93 ± 0.09, and 1.3 ± 0.1 ML, as determined by Rutherford backscattering spectrometry, were 0.07, 0.15, and 0.17 nm, respectively. The values are somewhat lower than the expected Sn thickness values of tetragonally distorted α-Sn films on Si. For Sn coverages of 0.49 ± 0.09, 0.93 ± 0.09, and 1.3 ± 0.1 ML, the expected values of the thickness for pseudomorphic and tetragonally distorted α-Sn on (100) Si are 0.090 ± 0.009, 0.17 ± 0.02, and 0.24 ± 0.02 nm, respectively. This discrepancy may be due to deviation of the Sn profile from a delta function profile, some nonsubstitutional Sn atom fraction, or local strain relaxation in the Si–Sn bond length.

This work was supported by the National Science Foundation and an Intel Graduate Fellowship (K.S.M.). The authors also acknowledge expert technical assistance from M. Easterbrook and C. Gardland, and C. Ahn, J. Christopherson, and R. Ragan for helpful discussions.

[1] S. Groves and W. Paul, Phys. Rev. Lett. **11**, 194 (1963).
[2] R. A. Soref and C. H. Perry, J. Appl. Phys. **69**, 539 (1991).
[3] H. A. Atwater, G. He, and K. Saipetch, Mater. Res. Soc. Symp. Proc. **355**, 123 (1995).
[4] G. He and H. A. Atwater, Phys. Rev. Lett. **79**, 1937 (1997).
[5] S. Yu. Shiryaev, J. Lundsgaard Hansen, P. Kringhoj, and A. Hylandsted Larsen, Appl. Phys. Lett. **67**, 2287 (1995).
[6] Al-S. T. Khan, P. R. Berger, F. J. Guarin, and S. S. Iyer, Appl. Phys. Lett. **68**, 3105 (1996).
[7] B. I. Craig, Superlattices Microstruct. **12**, 1 (1992).
[8] F. A. Trumbore, C. R. Isenberg, and E. M. Porbansky, J. Phys. Chem. Solids **9**, 60 (1959).
[9] H. P. Zeindl, T. Wegehaupt, I. Eisele, H. Oppolzer, H. Reisinger, G. Tempel, and F. Koch, Appl. Phys. Lett. **50**, 1164 (1987).
[10] W. Wegscheder, J. Olajos, U. Menczigar, W. Dondl, and G. Abstreiter, J. Cryst. Growth **123**, 75 (1992).
[11] D. J. Eaglesham, H.-J. Gossmann, and M. Cerullo, Phys. Rev. Lett. **65**, 1227 (1990).
[12] K. Ueda, K. Kinoshita, and M. Mannami, Surf. Sci. **145**, 261 (1984); D. H. Rich, T. Miller, A. Samsavar, H. F. Lin, and T.-C. Chiang, Phys. Rev. B **37**, 10 221 (1988); A. A. Baski and C. F. Quate, *ibid.* **44**, 11 167 (1991).

Downloaded 31 Aug 2006 to 131.215.240.9. Redistribution subject to AIP license or copyright, see http://apl.aip.org/apl/copyright.jsp